OPTIMIZATION OF FRICTION STIR WELDING PARAMETERS FOR SIMILAR AND DISSIMILAR ALUMINUM ALLOYS AA5083-H111 AND AA7075-T651

Azarias Mavropoulos[1*], Ioannis Tsikrikonis[2]

[1] Physical Metallurgy Laboratory, Dept. of Mechanical Engineering, Aristotle University of Thessaloniki, 541 24 Thessaloniki, Greece

[2] Hellenic Air Force, 110 Combat Wing, Larisa Air Base, Maintenance Squadron, Quality Assurance Office, Agias St, GR 41001, Larisa, Greece

Abstract

In recent years, the increasing demand in the industry for lightweight and durable materials has driven research into various aluminum alloys, which are relatively inexpensive and offer a high strength-to-weight ratio. Aluminum alloys are utilized across multiple sectors such as aerospace, automotive, and shipbuilding. Many applications require welding similar or dissimilar alloys, which, with conventional fusion methods, are often impossible or result in degraded weld quality. Friction Stir welding, a solid-state welding technique, is increasingly popular because it is eco-friendly, energy-efficient, and prevents common issues like solidification cracks. The goal of this work was to determine the optimal parameters for successful similar and dissimilar welds. Accordingly, three tools were designed and manufactured to perform butt welds on thin alloy plates of 5083-H111 and 7075-T651, both similar and dissimilar. The parameters were optimized, and the weld microstructure was examined using an optical microscope. Lastly, micro-hardness measurements were taken on the optimal welds.

Keywords: *friction stir welding, aluminum alloys, AA5083, AA7075, welding parameters*

1. INTRODUCTION

The friction stir welding technique was invented by Wayne Thomas in 1991 at the British Welding Institute (TWI), and it was found that the resulting welds were 90% error-free, with no melting of the materials as occurs in conventional fusion welding [1]. Today, there are more than 135 patents worldwide, and new techniques and applications are constantly being developed [2].

Friction stir welding is a solid-state welding technique because there is no melting of the materials being welded. The maximum temperature during welding reaches up to 90% of the melting temperature. According to the operating principle of friction stir welding, a rotating non-consumable tool consisting of a collar and a pin is inserted between the two edges of the materials to be welded. After the pin has penetrated to the appropriate depth and the materials have been sufficiently heated, it then moves in the direction of welding. During its movement, the friction of the collar and the intense plastic deformation caused by the pin locally increase the temperature. This results in the local “softening” of the materials, helping them to stir around the tool pin and transfer from the front of the tool to the back. As it moves, the tool exerts downward force through the flange, creating a permanent bond during the solidification of the materials [3]. Throughout the process, supporting the welding pieces properly on a suitable flat plate is important. The advantages of friction stir welding include [2-7] being a solid-state process that avoids the risk of solidification cracking, requiring less heat input than other fusion welding techniques and thus experiencing less solidification shrinkage, avoiding the formation of a fine recrystallized microstructure, offering improved mechanical properties, minimizing preparation of the welding surfaces, being applicable to all basic aluminum alloys, capable of performing overlay, butt, and spot welds, being environmentally friendly with no gas emissions, consuming low energy, and enabling repeatability and automation. The disadvantages are that it cannot be applied to all materials, especially those with high deformation resistance and high melting points; the pieces to be welded need good retention, and higher power is required for welding thicker pieces.

Koilraj et al. [8] studied butt welds between alloys 2219 T-87 and 5083-H321 by optimizing process parameters using the Taguchi method, focusing on ultimate tensile strength. Experimental results showed that the optimal parameters were 700 rpm rotation speed, 15 mm/min feed rate, and a flange-to-pin diameter ratio D/d = 3. The threaded cylindrical pin was found to perform better than the threaded, tapered, and unthreaded cylindrical pins. They also claimed that the flange-to-pin ratio accounts for 60% of the weld strength.

Saravanan et al. [9] performed welds on 2024 T-6 and 7075 T-6 to examine the effect of the flange-to-pin diameter ratio on the microstructure and mechanical properties of the weld. Given the remaining parameters, welds were made with ratios D/d = 2, D/d = 2.5, D/d = 3, D/d = 3.5, and D/d = 4 with the 2024-T6 placed on the advancing side. Their experiments showed that for a diameter ratio D/d = 3, there was maximum tensile strength, with an equal number of grooves indicating ductile fracture. For a diameter ratio D/d = 4, the weld had the lowest tensile strength. The microstructure of the stirring zone with a ratio of D/d = 3 confirmed the existence of a fine recrystallized structure, which was attributed to the small size of the flange diameter. This microstructure contributed to the good tensile strength.

Sadeesh et al. [10] used five different pin geometries (cylindrical, cylindrical with thread, square, tapered, tapered with thread) and two speed pairs (710 rpm rotation speed with 28 mm/min feed rate, 1000 rpm rotation speed with 40 mm/min feed rate) to weld 2024 T-4 and 6061 T-4 alloys. The study of the welds showed that the cylindrical threaded pin and the square pin produced defect-free welds. The cylindrical pin had a rotation speed of 710 rpm with a 28 mm/min feed rate, while the square pin used the second set of parameters (1000 rpm rotation speed with 40 mm/min feed rate). Among these two pins, the square pin performed welding with the best mechanical properties.

Unfried et al. [11] examined the impact of flange features on the microstructure development and mechanical properties of alloy 1100 welds. They analyzed three different flange bottom designs—flat bottom, concentric circle bottom, and spiral bottom—and measured the thermal cycling caused by each. The concentric circle and spiral designs were selected for their larger surface areas on the weld pieces compared to the flat bottom and to influence material flow. Specifically, the spiral feature had a 27% larger surface area than the flat bottom, while the concentric circle feature was 11% larger. Based on the remaining parameters, they determined that flange bottom designs induce less severe thermal cycling than the flat bottom. Additionally, the features resulted in different plasticity distributions due to their shapes and created a larger stirring zone with bigger grains compared to the flat bottom.

Moshwan et al. [12] welded 5052-O alloy at rotational speeds of 800 rpm, 1000 rpm, 1500 rpm, 2000 rpm, and 3000 rpm and measured the forces exerted on the tool, given the remaining parameters. They also observed the microstructure of the weld. From the observation of the welds, they concluded that all rotational speeds successfully welded the materials except 3000 rpm. The optimal weld in terms of tensile strength was that with a rotational speed of 1000 rpm. Furthermore, the dissolution of intermetallic compounds in the stirring zone degraded the mechanical properties of the weld. In addition, they observed that with increasing rotational speed, the axial force decreased and the longitudinal force increased, while the influence on the transverse force was insignificant.

Kundu et al. [13] welded 5083 and 5086 alloys. The experiments were performed at various speeds, tool rake angles, and pin profiles. The weld performance was examined and compared with the base metals. Their observations showed that the pin geometry affects the material flow, and the stirring conditions are different for cylindrical and square pins. The surface quality is affected by the tool rake angle, and discontinuities increase with increasing angle. The tensile strength increases with increasing rotational speed, feed rate, and tool rake angle up to a point and then decreases.

Gu et al. [14] welded 5086-H32 alloys with a tapered pin at a rotation speed of 1600 rpm and feed rates of 175 mm/min, 200 mm/min, and 225 mm/min, respectively. They then examined the microstructure and mechanical properties. The results of their experiments showed that with feed rates of 200 mm/min and 225 mm/min, a small amount of porosity was created in the weld, and the presence of oxides was found. At a speed of 175 mm/min, the porosity was increased. The optimum feed rate was 200 mm/min with a tensile strength of the weld of 75% of the base metal and a ductility of 25%. This tensile strength value was attributed to the loss of some of the cold workability in the stir zone with the heat input during welding, combined with the presence of oxides. The low ductility was also attributed to the presence of oxides and loss of tensile strength.

Bahemmat et al. [15] performed weld tests on 7075 T-6 alloys with a tapered threaded pin and a threaded pin with four (4) grooves. The feed rate was 80 mm/min, and the axial force on the tool was 10 kN. The welds without defects had rotation speeds of 900 rpm for the tapered pin and 700 rpm for the grooved pin. The tapered pin produced a weld with a higher elongation and lower tensile strength compared to the grooved pin. The average hardness of the stir zone in both (2) pin cases decreased with increasing rotation speeds. The fracture initiation region of the welds without defects was located close to the areas of reduced hardness on the retreat side.

Saeidi et al. [16] welded dissimilar alloys 7075 T-6 and 5083-H116 using a square pin. The highest tensile strength was obtained with those produced at rotational speeds of 500 rpm or 800 rpm and a feed rate of 50 mm/ min. A mathematical model used showed a good relationship between these parameters and tensile strength, with a maximum error of 1%. Its optimization showed that the highest tensile strength was obtained with welding at a rotational speed of 500 rpm.

2. MATERIALS AND METHODS

The materials used to perform the welds were aluminum alloys 5083-H111 and 7075-T651. Their dimensions were 130mm × 23mm × 5mm.

The FIRST milling machine, model LC-1 ½ VS, manufactured in Taiwan, was used to perform the welds. This milling machine can develop rotation speeds of 50rpm-3750rpm.

The welding tools were made of heat-treated tool steel. More specifically, the material used was Orvar. Supreme. Its chemical composition is similar to that of AISI H 13 [17]. In order to increase the resistance of the tools to breakage, an appropriate heat treatment was selected to obtain a hardness of 53 HRC. The heat treatment that the tools underwent included austenitization at 1025 o C for 30 minutes, air painting, and two annealings at 570 ^{o}C for two hours, with intermediate cooling to room temperature [17].

Following a literature search, three tools with a cylindrical outer flange surface were chosen for construction. The pin profiles chosen to be manufactured are cylindrical, square, and truncated conical. All pin profiles have a flat bottom. As pin characteristics, a thread with a depth of 0.5 mm and a pitch of 1 mm was chosen for the cylindrical and conical pins. The conical pin has a concave profile flange with an angle of 10°, while the cylindrical and square pins have flat profile flanges. Drawing 1 presents the construction drawings of the three tools.

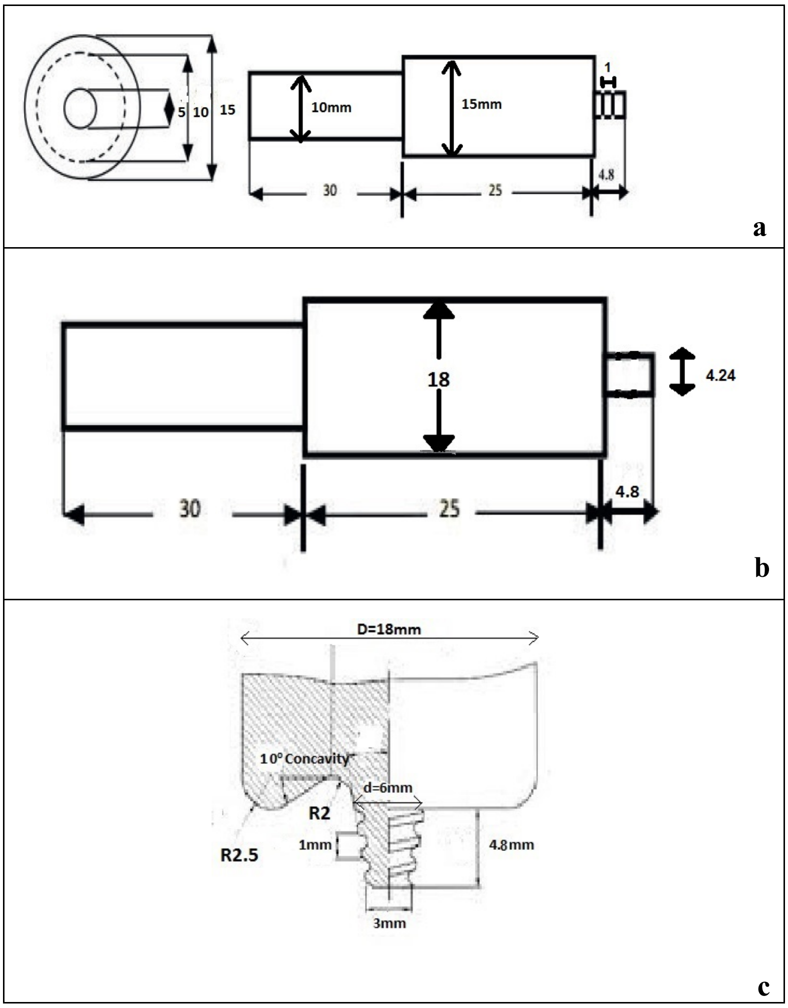

Drawing 1. Construction drawings of a) cylindrical, b) square, c) conical pin

All welds were performed perpendicular to the rolling direction of the pieces. In the welds of the two dissimilar alloys, the alloy 7075-T651 was chosen to be placed on the advancing side, following the usual practice that the stronger metal is placed on the advancing side.

3. RESULTS AND DISCUSSION

Similar and dissimilar welds were performed, under various conditions and with the three welding pins in order to optimize the welding parameters. Table 1 presents the parameters that give us the optimal welds.

Welding materials	Rotation Speed (rpm)	Feed Speed (mm/min)	Tool tilt	Welding pin type
Similar alloys 5083- H 111	2330	19	3°	conical
Similar alloys 7075- T 651	2000	28	3°	conical
Dissimilar alloys 7075-T651 and 5083-H111	1400	22	3°	conical

Table 1. Optimal parameters for performing similar and dissimilar welds

Figure 1 shows the external view of a similar weld of alloy 5083-H111. The external appearance of both sides of the weld is good, and no material overflow was observed.

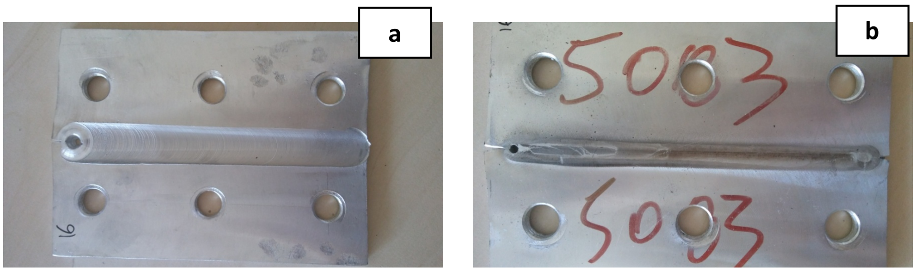

Fig. 1. (a) Top and (b) bottom views of a similar weld AA5083-H 111

With the above welding conditions, no defects were found in the weld section. In the right part of Figure 2a, the fine grains of the stirring zone are visible, while in the left part, the grains are strongly deformed and belong to the thermomechanically affected zone. Similarly, in the left part of Figure 2b, the fine grains of the stirring zone are visible, while in the right part of the image, the deformed grains of the thermomechanically affected zone are visible. The grains of the stirring zone are fine, without orientation, and their boundaries are indistinct. Dynamic recrystallization prevails as the main phenomenon that shapes their size. The boundary separating the stirring zone and the thermomechanically affected zone is clearly visible on the advancing side in contrast to the retreating side, where it is noticeable by observing the differences in grain sizes.

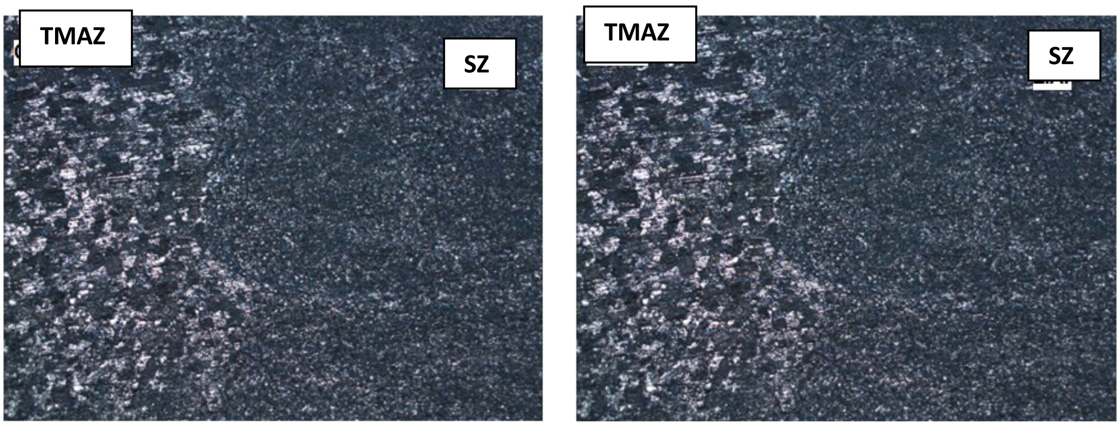

Fig. 2. a) Separation of stirring zone (SZ) and thermomechanically affected zone (TMAZ) on the advancing side of similar weld 5083- H 111, optical microscope, magnification ×50 b) Separation of the stirring zone (SZ) and the thermomechanically affected zone (TMAZ) on the retreat side of a similar weld 5083- H 111, optical microscope, magnification ×50

The microstructure of the base metal and the heat-affected zone is shown in Figure 3. It is evident that the grain size of the heat-affected zone has increased due to the thermal cycling that the zone undergoes.

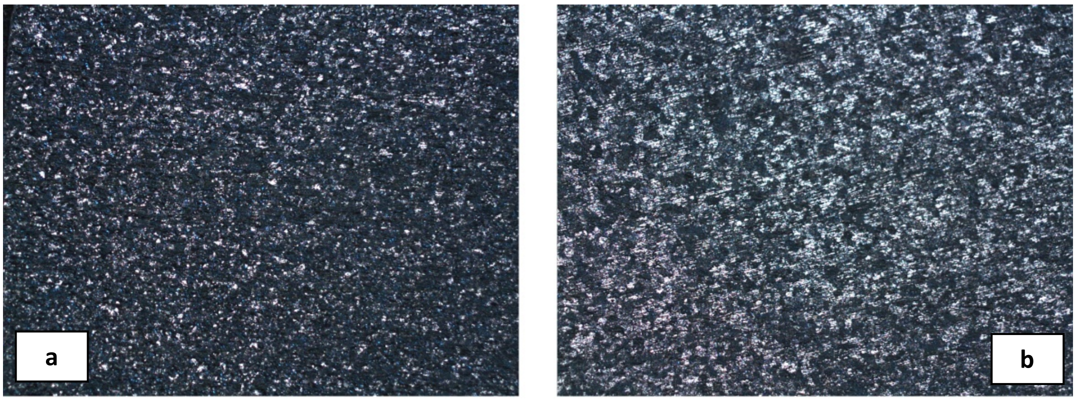

Fig. 3. Microstructure of (a) Base metal and (b) Heat affected zone of a similar weld 5083-H111, optical microscope, magnification ×50

Figure 4 shows the top and bottom views of a similar weld of alloy 7075-T651. Externally, the two views are satisfactory, and no errors were found in the vertical sections.

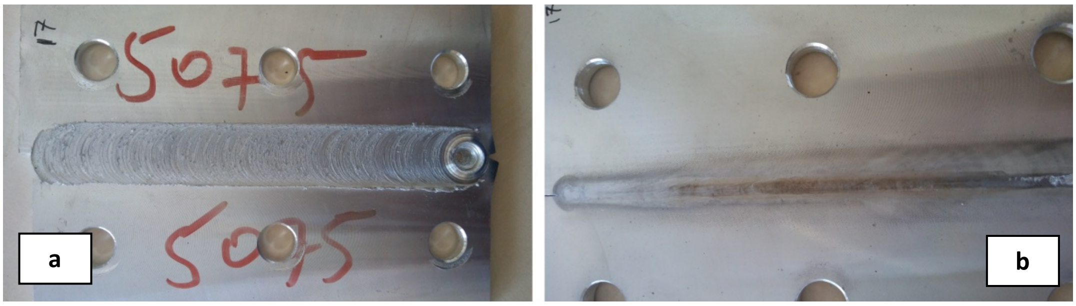

Fig. 4. (a) Top view and (b) bottom view of a similar weld of alloy AA7075-T651

Figure 5a shows the boundary between the stirring zone and the thermomechanically affected zone (left part of the image) for the advancing side. The corresponding boundary between the two zones is shown in Figure 5b for the retreating side (the intense blue area between the two zones is due to chemical attack).

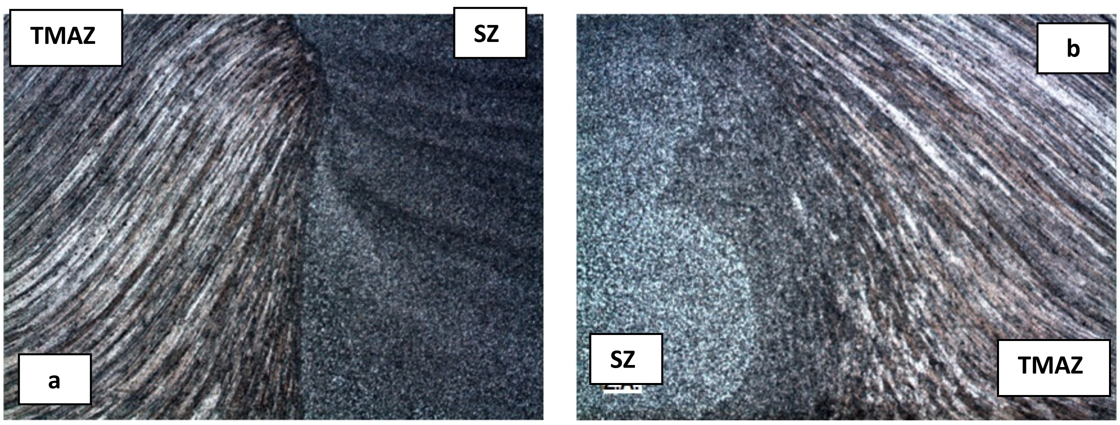

Fig. 5. a) Separation of the stirring zone (SZ) and the thermomechanically affected zone (TMAZ) of the advancing side of a similar weld 7075- T651, optical microscope, magnification ×50, b) Separation

of the stirring zone (SZ) and the thermomechanically affected zone (TMAZ) of the retreating side of a similar weld 7075- T 651, optical microscope, magnification ×50

Figure 6 shows the external view of a dissimilar weld of alloys 7075-T651 and 5083-H111. No errors were found in the sections that were made, and the external views of the weld are satisfactory.

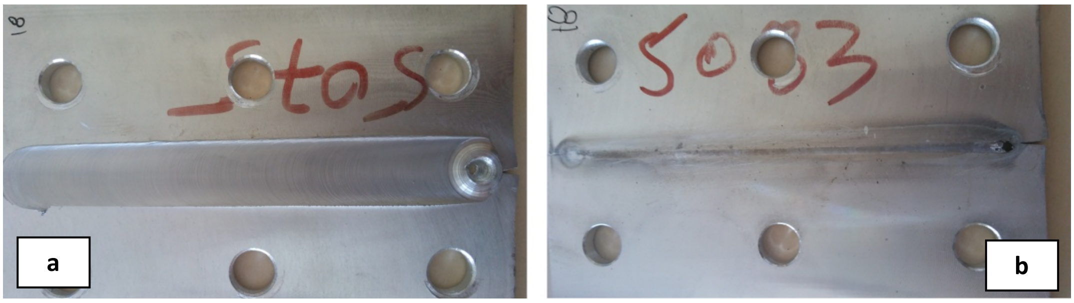

Fig. 6. (a) Top and (b) Bottom view of dissimilar weld 5083-H111 and 7075-T651

Figure 7 shows the separation of the stirring zone from the thermomechanically affected zone for both sides of the weld. On the advancing side, the boundary is evident, while on the retreating side it is quite indistinct. Essentially, it is only noticeable from the change in grain size, as in the left part of Figure 7b, the grains are fine, while in the right part, the grains are larger (the black parts are 7075-T651 material belonging to the stirring zone). From Figure 7a, it is evident that the grains of the stirring zone are fine, recrystallized, and without orientation.

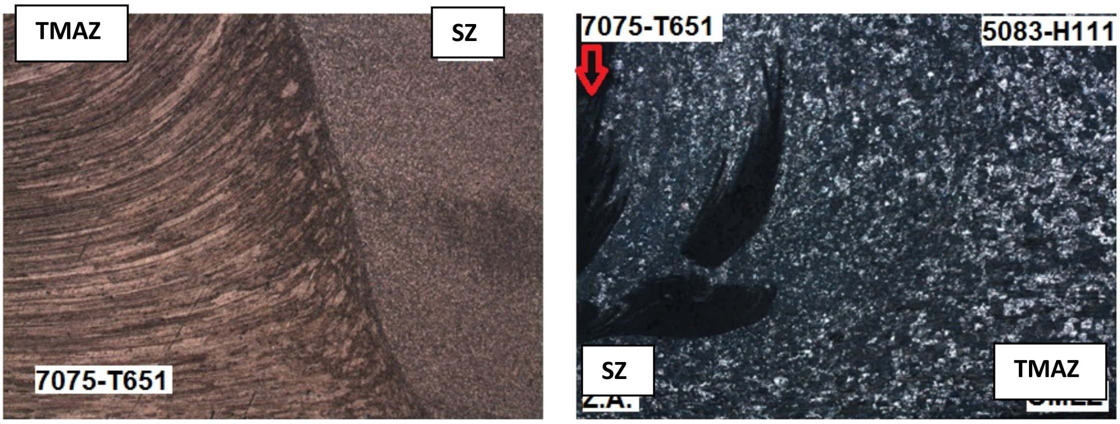

Fig. 7. a) Separation of the stirring zone (SZ) and the thermomechanically affected zone (TMAZ) on the advancing side of the dissimilar weld 5083-H111 and 7075-T651, optical microscope, magnification ×50, b) Separation of the stirring zone (SZ) and the thermomechanically affected zone (TMAZ) on the retreating side of the dissimilar weld 5083- H111 and 7075- T651, optical microscope, magnification ×50

3.1 Microhardness measurements of welds of similar and dissimilar alloys

Figure 8a shows the microhardness measurements of a similar weld of alloy AA5083-H111. From the diagram, it becomes clear that the microhardness has decreased in the weld zones compared to the base metal. This is due to the loss of cold workability, as the thermal cycle of welding affects the specific alloy, similar to annealing, in the intrahardened state (H111). The partial recovery of the microhardness in the stir zone compared to the thermomechanically affected zones is due to grain refinement.

Figure 8b presents the results of microhardness measurements of a similar weld of alloy AA 7075-T651. From the diagram it becomes clear that the microhardness has decreased in the weld zones in relation to the base metal. This is most likely due to dissolution phenomena and/or enlargement of the reinforcing phase in the weld zones. The partial recovery of the microhardness in the stirring zone compared to the rest is due to grain refinement. The lower values are observed in the heat affected zones.

Figure 8c shows the microhardness values of dissimilar welds 5083-H111 and 7075-T651. Similar to the previous cases, a decrease in microhardness is observed compared to the base metals. For alloy 7075-T651 on the advancing side, in the thermomechanically affected zone, the microhardness decreases probably as a result of partial dissolution of the reinforcing phase, while in the heat-affected zone, it decreases as a result of the enlargement of the reinforcing phase by the thermal cycle of welding. For alloy 5083-H111, in the thermomechanically affected zone and the heat-affected zone, the microhardness decreases due to the annealing caused by the thermal cycle. The large value (~287) at the boundary of the stirring zone may correspond to a bimetallic compound.

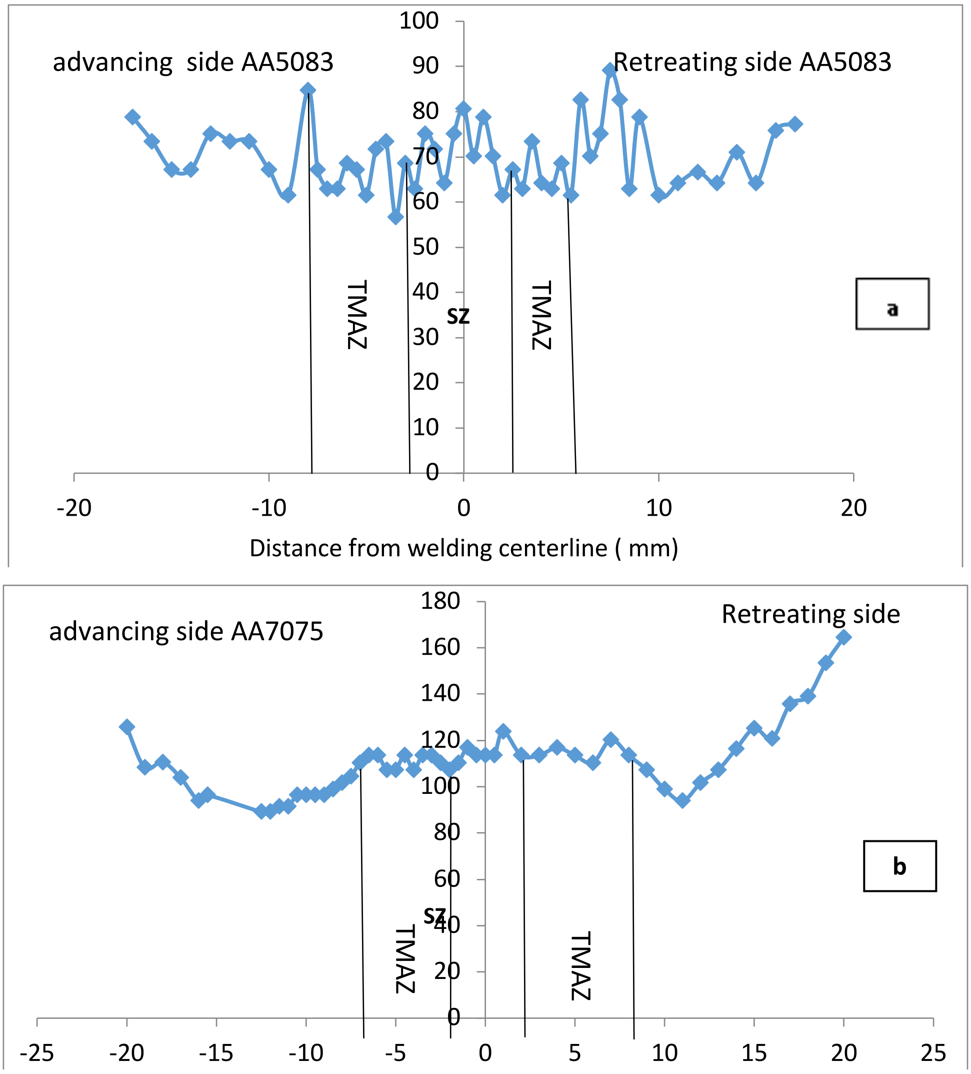

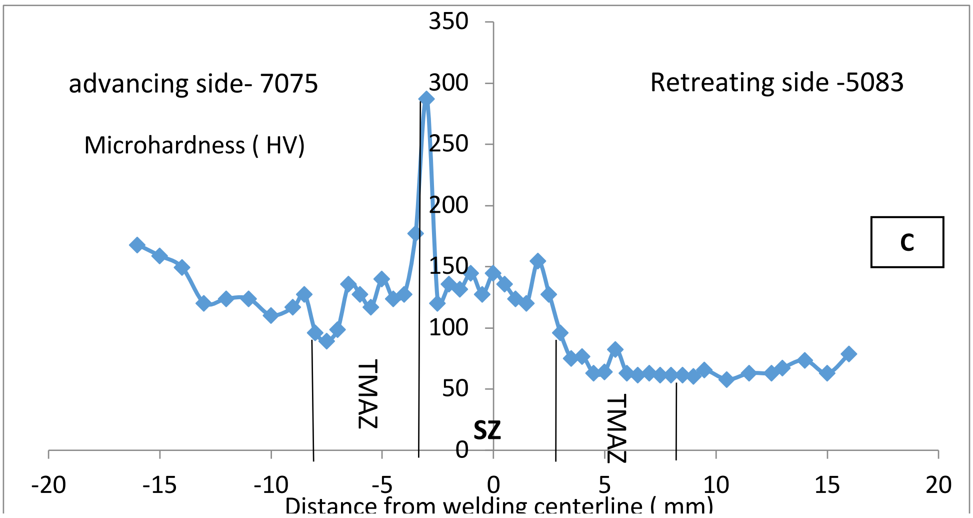

Fig. 8. Vickers microhardness measurements a) of similar weld of alloy AA5083-H111, b) of similar weld of alloy AA7075-T651, c) of dissimilar weld of alloys AA7075-T651 and AA5083-H111

4. CONCLUSIONS

The experiments showed that a simple milling machine can perform friction and stirring welds. However, their quality depends on the experience of the user.

From the conduct of the experiments, it became apparent that adequate containment of the specimens is of crucial importance for the elimination of discontinuity errors and material overflow.

In all of the welds carried out, the reduction in errors was achieved by increasing the rotational speed.

The tool with the tapered pin and the concave profile flange produced the best welds compared to the other pins.

In the welds performed (similar or dissimilar), the microhardness is reduced in all their zones compared to the base metal.

In similar welds, the stirring zone consists of a fine-grained microstructure where the grain size decreases from the upper part to the lower part.

In similar welds, microhardness values show a slight increase in the stirring zone compared to the other zones due to the grain refinement in this zone.

In the welds carried out, it was found that by increasing the rotational speed, the errors are either limited or eliminated. However, increasing the rotational speed significantly increases the heat input to the weld, which changes the microstructure, resulting in a degradation of its mechanical properties. Therefore, controlling the heat input is of crucial importance in optimizing the microstructure and mechanical properties of the weld.

REFERENCES

1. Thomas, WM, Nicholas, ED, Needham, JC, Murch, MG, Templesmith, P., & Dawes, CJ (1991). GB Patent application no. 9125978.8. In *International Patent Application No. PCT/GB92/02203*.
2. Marathe, SP (2017). *a Review Paper on: Friction Stir Welding (Fsw)*. *3* (March 2016), 1403–1406.
3. Mishra, RS, Mahoney, MW, & Company, RS (2007). *Chapter 1* . https://doi.org/10.1361/fswp2007p001

4. Çam, G., & Mistikoglu, S. (2014). Recent developments in friction stir welding of aluminum alloys. *Journal of Materials Engineering and Performance*, *23* (6), 1936–1953. https://doi.org/10.1007/s11665-014-0968-x
5. Threadgill, PL, Leonard, AJ, Shercliff, HR, & Withers, PJ (2009). Friction stir welding of aluminum alloys. *International Materials Reviews*, *54* (2), 49–93. https://doi.org/10.1179/174328009X411136
6. Jain, S., Bhuva, K., Patel, P., & Badheka, V.J. (2019). A review on dissimilar friction stir welding of aluminum alloys to titanium alloys. *Advances in Intelligent Systems and Computing*, *757* (1), 415–425. https://doi.org/10.1007/978-981-13-1966-2_37
7. Prashant Pratap Mall, & Jitender Panchal. (2017). Friction Stir Welding Process Parameters: A Review. *International Journal of Engineering Research And V6* (06). https://doi.org/10.17577/ijertv6is060029
8. Koilraj, M., Sundareswaran, V., Vijayan, S., & Koteswara Rao, SR (2012). Friction stir welding of dissimilar aluminum alloys AA2219 to AA5083 - Optimization of process parameters using Taguchi technique. *Materials and Design*, *42*, 1–7. https://doi.org/10.1016/j.matdes.2012.02.016
9. Saravanan, V., Rajakumar, S., Banerjee, N., & Amuthakkannan, R. (2016). Effect of shoulder diameter to pin diameter ratio on microstructure and mechanical properties of dissimilar friction stir welded AA2024-T6 and AA7075-T6 aluminum alloy joints. *International Journal of Advanced Manufacturing Technology*, *87* (9–12), 3637–3645. https://doi.org/10.1007/s00170-016-8695-0
10. Sadeesh, P., Venkatesh, KM, Rajkumar, V., Avinash, P., Arivazhagan, N., Devendranath, RK, & Narayanan, S. (2014). Studies on friction stir welding of AA 2024 and AA 6061 dissimilar metals. *Procedia Engineering*, *75*, 145–149. https://doi.org/10.1016/j.proeng.2013.11.031
11. Unfried-Silgado, J., Torres-Ardila, A., Carrasco-García, JC, & Rodríguez-Fernández, J. (2017). Effects of the shoulder geometry of the tool on microstructure and mechanical properties of friction stir welded joints of AA1100 aluminum alloy. *Dyna* , *84* (200), 202–208. https://doi.org/10.15446/dyna.v84n200.55787
12. Moshwan, R., Yusof, F., Hassan, MA, & Rahmat, SM (2015). Effect of tool rotational speed on force generation, microstructure, and mechanical properties of friction stir welded Al-Mg-Cr-Mn (AA 5052-O) alloy. *Materials and Design*, *66* (PA), 118–128. https://doi.org/10.1016/j.matdes.2014.10.043
13. Kundu, J., & Singh, H. (2016). Friction stir welding of dissimilar Al alloys: Effect of process parameters on mechanical properties. *Engineering Solid Mechanics*, *4* (3), 125–132. https://doi.org/10.5267/j.esm.2016.2.001
14. Gu, S., & Serindag, HT (2009). *Mechanical properties of friction stir butt-welded*. *8* . https://doi.org/10.1002/mawe.200800455
15. Bahemmat, P., Besharati, MK, Haghpanahi, M., Rahbari, A., & Salekrostam, R. (2009). *Mechanical, micro-, and macrostructural analysis of AA7075 – T6 fabricated by friction stir butt welding with different rotational speeds and tool pin profiles*. *224*, 419–433. https://doi.org/10.1243/09544054JEM1554
16. Saeidi, M., Manafi, B., Givi, M.K.B., & Faraji, G. (2015). *Mathematical modeling and optimization of friction stir welding process parameters in AA5083 and AA7075 aluminum alloy joints*. https://doi.org/10.1177/0954405415573697
17. Uddeholm. (2013). *Uddeholm Orvar Supreme*. Datasheet